THE ASTROPHYSICAL JOURNAL, 464:L11–L15, 1996 June 10

POWER SPECTRUM OF PRIMORDIAL INHOMOGENEITY DETERMINED FROM THE FOUR-YEAR *COBE*[1] DMR SKY MAPS

K. M. GÓRSKI,[2,3,4] A. J. BANDAY,[2,5] C. L. BENNETT,[6] G. HINSHAW,[2] A. KOGUT,[2] G. F. SMOOT,[7] AND E. L. WRIGHT[8]
Received 1996 January 9; accepted 1996 March 21

ABSTRACT

Fourier analysis and power spectrum estimation of the cosmic microwave background anisotropy on an incompletely sampled sky developed by Górski has been applied to the 4 yr *COBE* DMR 31.5, 53, and 90 GHz sky maps. Likelihood analysis using newly constructed Galaxy cuts (extended beyond $|b| = 20°$ to excise the known foreground emission) and simultaneously correcting for the faint high-latitude Galactic foreground emission is conducted on the DMR sky maps pixelized in both ecliptic and Galactic coordinates. The Bayesian power spectrum estimation from the foreground-corrected 4 yr *COBE* DMR data renders $n \sim 1.2 \pm 0.3$ and $Q_{\rm rms-PS} \sim 15.3^{+3.7}_{-2.8}$ μK (projections of the two-parameter likelihood). The results are consistent with the Harrison-Zeldovich $n = 1$ model of amplitude $Q_{\rm rms-PS} \sim 18$ μK detected with significance exceeding 14 σ ($\delta Q/Q \gtrsim 0.07$). (A small power spectrum amplitude drop below the published 2 yr results is predominantly due to the application of the new, extended Galaxy cuts.)

Subject headings: cosmic microwave background — cosmology: observations — large-scale structure of universe — methods: analytical — methods: statistical

1. INTRODUCTION

Following the seminal *COBE* DMR discovery of the anisotropy of the cosmic microwave background (CMB) after 1 yr (1989/1990) of observations (Smoot et al. 1992; Bennett et al. 1992; Wright et al. 1992; Kogut et al. 1992) the instrument continued operating until late 1993. Intermediate, 2 yr results of the mission were reported by Bennett et al. (1994; see also, e.g., Górski et al. 1994 and Wright et al. 1994). A summary of the 4 yr results is provided by Bennett et al. (1996). In this Letter we apply the CMB anisotropy power spectrum estimation technique introduced by Górski (1994) to the definitive, 4 yr 31.5, 53, and 90 GHz sky maps resulting from the *COBE* DMR mission.

The *COBE* DMR-detected anisotropy of the CMB provides a unique opportunity to measure the spatial distribution of the inhomogeneities in the universe on the comoving scales ranging from a few hundred Mpc up to the present horizon size (inaccessible to any other astronomical observations) during the embryonic stage of their evolution, thereby avoiding the complications of (cosmologically) recent evolution of most astrophysical systems. There are, however, important experimental/observational limitations on the extent to which cosmologically interesting quantities can be extracted from the DMR data. These are imposed by our understanding of systematic effects, instrumental noise properties, and noncosmological foreground signals peculiar to our location in the Galaxy and in the universe. Kogut et al. (1996c) have addressed systematic effects in considerable detail and found them to be unimportant relative to the accuracy to which cosmological parameters can be determined from the DMR 4 yr data. Górski et al. (1996) describe the noise properties of the DMR sky maps and demonstrate the sufficiency of the DMR noise models (see also Lineweaver et al. 1994). Emission from the Galactic plane cannot be modeled to adequate precision and must be excised from the data (see § 2 and Banday et al. 1996a). Foreground Galactic emission at high latitude (Bennett et al. 1992; Kogut et al. 1996a, 1996b) can be partially accounted for by using Galaxy-dominated spatial templates at frequencies where the CMB does not dominate (see § 3, and Kogut et al. 1996a, 1996b). The potential contamination of the CMB anisotropy by the astrophysical foregrounds outside of our Galaxy is demonstrated to be negligible in Banday et al. (1996b).

In this Letter we focus on a general characterization of the 4 yr DMR sky maps in terms of a power spectrum of the angular distribution of the CMB temperature fluctuations and estimate its sensitivity to a plausible foreground emission contamination. We use and further develop the method introduced by Górski (1994, hereafter G94a) and applied to the 2 yr DMR data in Górski et al. (1994, hereafter G94b). In the likelihood analysis we utilize a power-law family of model power spectra specified by $Q_{\rm rms-PS}$ and n—the amplitude and shape parameters (Bond & Efstathiou 1987; Fabbri, Lucchin, & Matarrese 1987), but we often abbreviate the symbol $Q_{\rm rms-PS}$ and use Q instead. The results of the analysis involving the CMB spectra of specific large-scale structure models will be presented elsewhere. Hereafter, bold letters denote matrices (*uppercase*) and vectors (*lowercase*), and p is a pixel label.

2. DATA

Our published analysis of the 2 yr DMR data (G94b) involved a simple $|b| > 20°$ Galaxy cut, which retained the

[1] The National Aeronautics and Space Administration/Goddard Space Flight Center (NASA/GSFC) is responsible for the design, development, and operation of the *Cosmic Background Explorer* (*COBE*). Scientific guidance is provided by the *COBE* Science Working Group. GSFC is also responsible for the analysis software and for the production of the mission data sets.

[2] Hughes STX Corporation, Laboratory for Astronomy and Solar Physics, Code 685, NASA/GSFC, Greenbelt, MD 20771.

[3] On leave from Warsaw University Observatory, Aleje Ujazdowskie 4, 00-478 Warsaw, Poland.

[4] E-mail: gorski@stars.gsfc.nasa.gov.

[5] Max-Plank-Institut für Astrophysik, Karl-Swarzschild-Strasse 1, 85740 Garching bei München, Germany.

[6] Laboratory for Astronomy and Solar Physics, Code 685, NASA/GSFC, Greenbelt, MD 20771.

[7] Department of Physics, Lawrence Berkeley Laboratory, Space Sciences Laboratory, and Center for Particle Astrophysics, Building 50-351, University of California, Berkeley, CA 94720.

[8] UCLA Astronomy, P.O. Box 951562, Los Angeles, CA 90095-1562.

relatively bright foreground emission from the Scorpius-Ophiucus and Taurus-Orion regions (de Vaucouleurs 1955). In this work we employ new, extended Galactic cuts (see Banday et al. 1996a), which further excise these regions from the data used for the inference of the cosmological CMB anisotropy. We consider both extended $|b| > 20°$ (denoted 20+) and extended $|b| > 30°$ (30+) Galaxy cuts. We analyze the DMR sky maps in both ecliptic (E) and Galactic (G) pixelization. To facilitate a comparison of the 4 yr results with the published analyses of the 2 yr data we reapply the simple $|b| > 20°$ Galaxy cut. From a total of 6144 data pixels on the entire sky, the following numbers of pixels remain for analysis after applying the different Galactic cuts: 4038 for E20, 4016 for G20, 3890 for E20+, 3881 for G20+, 3039 for E30+, and 3056 for G30+.

We form weighted average maps at each frequency by combining the A and B channels:

$$\begin{aligned} \Delta_{31} &= 0.611\Delta_{31A} + 0.389\Delta_{31B}, \\ \Delta_{53} &= 0.579\Delta_{53A} + 0.421\Delta_{53B}, \\ \Delta_{90} &= 0.382\Delta_{90A} + 0.618\Delta_{90B}, \end{aligned} \tag{1}$$

minimizing the cut-sky–averaged noise variance pixel^{-1} in the combined maps. The weighted 31.5, 53, and 90 GHz 4 yr cut-sky DMR maps are analyzed jointly (equivalent to co-addition) with and without the foreground correction, or linearly combined (after foreground correction, indicated by tilde) with the weights designed to remove any leftover free-free emission:

$$\tilde{\Delta}_{\rm CMB} = -0.302\tilde{\Delta}_{31} + 0.633\tilde{\Delta}_{53} + 0.669\tilde{\Delta}_{90}. \tag{2}$$

The weights given to both 31.5 and 90 GHz maps in this linear combination technique are considerably larger than those in the co-added technique (~0.08 and ~0.26, respectively). As a result, the noise is larger in the linear combination map $\tilde{\Delta}_{\rm CMB}$, slightly exceeding the rms noise in the 90 GHz map alone.

Fourier analysis of the cut-sky maps is performed (see G94a for details) in the 961-dimensional linear space spanned by the orthonormal functions $\boldsymbol{\psi}$, which are linear combinations of spherical harmonics with $\ell \le 30$. A sky map at frequency ν, $\Delta_\nu(p)$ (where p is the pixel label) is Fourier decomposed as follows:

$$\begin{aligned} c_{i,\nu} &= \frac{4\pi}{6144} \sum_{p\in\{\text{cut sky}\}} \Delta_\nu(p)\psi_i(p), \\ \Delta_\nu(p)|_{p\in\{\text{cut sky}\}} &= \boldsymbol{c}_\nu^T \cdot \boldsymbol{\psi}(p). \end{aligned} \tag{3}$$

Fourier coefficients c_i are linear in pixel temperatures and account for the cut-sky mode coupling explicitly. Figure 1 (Plate L6) displays an example of the $\boldsymbol{\psi}$ basis function constructed for various versions of the Galaxy cut used in this work.

The dominant component (in rms pixel^{-1}) of the raw, dipole-subtracted, cut-sky DMR maps is the instrument-generated noise. A correct statistical modeling of this contaminant is essential for any method attempting to quantify the cosmological CMB anisotropy. A detailed analysis of noise properties of the entire DMR data set is discussed in Górski et al. (1996). Here we employ the noise modeling in Fourier space as described in G94a and G94b. The noise content of the 4 yr DMR data is characterized by the rms noise amplitudes per Fourier mode of approximately 10.5, 3.4, and 5.5 μK at 31.5, 53, and 90 GHz, respectively. The co-addition of all available measurements at three frequencies renders a map with the rms noise amplitude per Fourier mode of ~2.7 μK.

3. LIKELIHOOD ANALYSIS OF FOREGROUND-CORRECTED DMR SKY MAPS

Following G94a and G94b, we conduct Bayesian inference from the *COBE* DMR data of the power spectrum of primordial CMB anisotropy under the usual assumption that the measurement [here the joint vector of coefficients of Fourier decomposition of the 31.5, 53, and 90 GHz sky maps, $\hat{\boldsymbol{c}}_\Psi^T \equiv (\hat{\boldsymbol{c}}_{31}^T, \hat{\boldsymbol{c}}_{53}^T, \hat{\boldsymbol{c}}_{90}^T)$] is a sum of a signal (primordial CMB anisotropy) and noise (a random, receiver-generated contamination) and that both these components are Gaussian stochastic variables. Hence, the likelihood function is an *exact* multivariate Gaussian in variable $\boldsymbol{c}_\Psi$. The likelihood density is fully specified by the Fourier space correlation matrices of signal, $\boldsymbol{C}_S$, a function of the assumed (and tested) power spectrum of the CMB anisotropy, and noise (at a given frequency ν), $\boldsymbol{C}_{N_\nu}$, which are are computed as described in G94a and G94b. No approximations or Monte Carlo simulations are required for evaluation of the likelihood function, and this power spectrum parameter estimation technique, bilinear in the measurement values of temperature perturbations, is statistically unbiased.

This formulation of the likelihood problem allows one naturally to address a problem of contamination of the CMB anisotropy data by the diffuse foreground emission. Assume (generally) that the anisotropy $\boldsymbol{c}_\nu$ is measured at M frequencies ν, and the foreground emission can be measured or modeled as a certain number N of nonstochastic spatial templates $F_k(p)$ (whose Fourier transforms are $\boldsymbol{f}_k$, $k = 1, \ldots, N$). The template-corrected joint data vector $\tilde{\boldsymbol{c}}_\Psi$ and its covariance matrix $\boldsymbol{C}_{\rm SN\Psi}$ are

$$\begin{aligned} \tilde{\boldsymbol{c}}_\Psi &= \begin{pmatrix} \hat{\boldsymbol{c}}_{\nu_1} - \sum_{k=1}^{k=N} \alpha_{\nu_1}^k \boldsymbol{f}_k \\ \cdots \\ \hat{\boldsymbol{c}}_{\nu_M} - \sum_{k=1}^{k=N} \alpha_{\nu_M}^k \boldsymbol{f}_k \end{pmatrix}, \\ \boldsymbol{C}_{\rm SN\Psi} &= \langle \tilde{\boldsymbol{c}}_\Psi \cdot \tilde{\boldsymbol{c}}_\Psi^T \rangle = \begin{pmatrix} \boldsymbol{C}_{{\rm SN}_{\nu_1}} & \cdots & \boldsymbol{C}_S \\ \cdots & \cdots & \cdots \\ \boldsymbol{C}_S & \cdots & \boldsymbol{C}_{{\rm SN}_{\nu_M}} \end{pmatrix}, \end{aligned} \tag{4}$$

where the matrix $\boldsymbol{C}_{{\rm SN}_{\nu_i}} = \boldsymbol{C}_S + \boldsymbol{C}_{N_{\nu_i}}$ specifies the Gaussian probability distribution of the receiver noise contaminated theoretical CMB anisotropy signal at a given frequency ν_i. With these definitions the likelihood function takes the usual form

$$P(\tilde{\boldsymbol{c}}_\Psi) \propto \exp\left(-\tilde{\boldsymbol{c}}_\Psi^T \cdot \boldsymbol{C}_{\rm SN\Psi}^{-1} \cdot \tilde{\boldsymbol{c}}_\Psi/2\right) / \sqrt{\det \boldsymbol{C}_{\rm SN\Psi}}. \tag{5}$$

This is a function of all parameters used to describe the CMB power spectrum and $M \times N$ coefficients α_ν^k used in the foreground correction. For a given CMB power spectrum (i.e., a fixed $\boldsymbol{C}_S$) the likelihood can be maximized with respect to parameters α_ν^k as a usual χ^2 fitting problem (dimension of the data vector is presumed large compared to both M and N). From the maximum likelihood equations, $\partial \ln P/\partial \alpha_\nu^k = 0$, one derives the following set of linear equations (for a given ν and k):

$$\sum_{j,\nu'} \boldsymbol{f}_k^T \cdot (\boldsymbol{C}_{\rm SN\Psi}^{-1})_{\nu\nu'} \cdot \boldsymbol{f}_j \alpha_{\nu'}^j = \sum_{\nu''} \boldsymbol{f}_k^T \cdot (\boldsymbol{C}_{\rm SN\Psi}^{-1})_{\nu\nu''} \cdot \hat{\boldsymbol{c}}_{\nu''}, \tag{6}$$

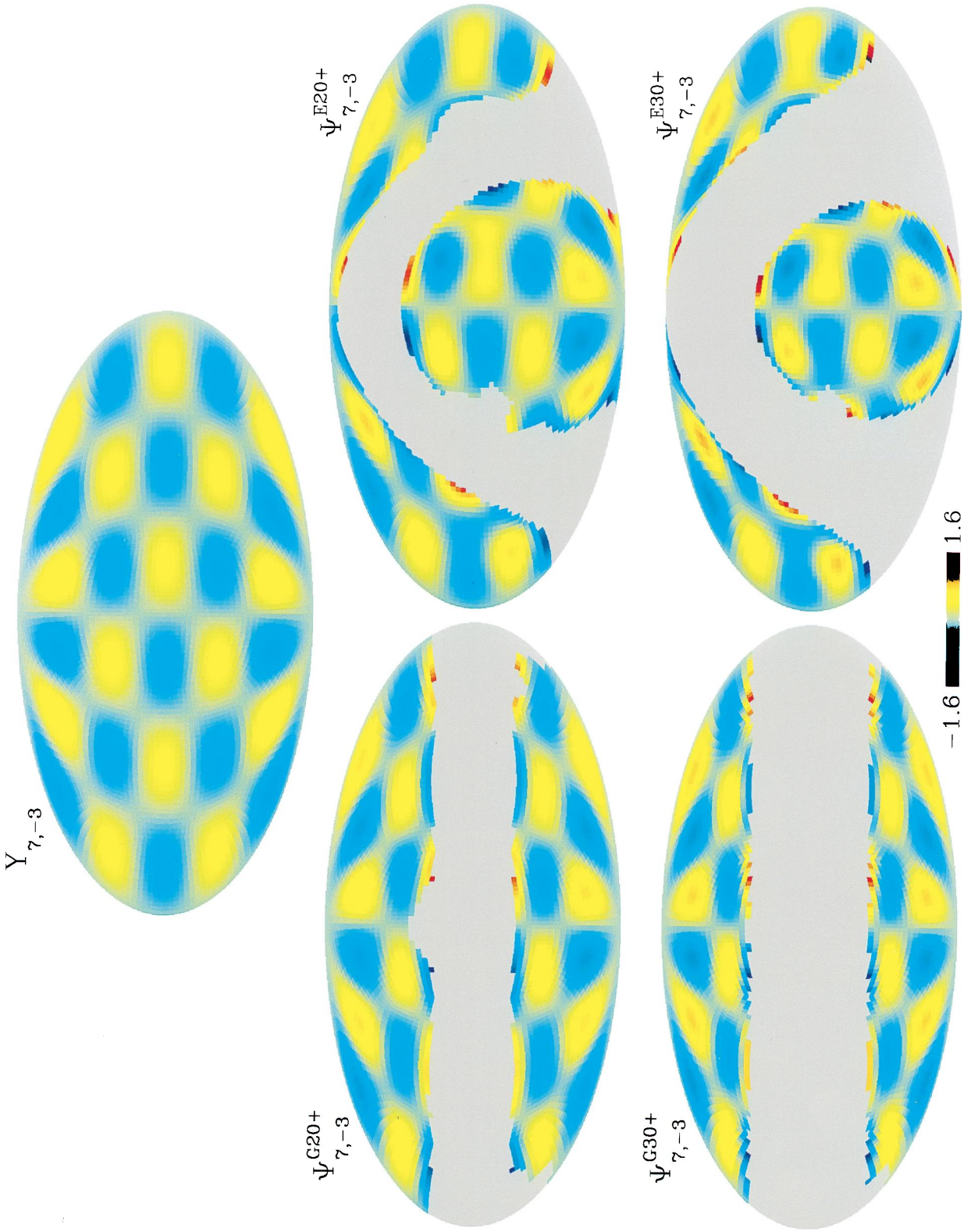

FIG. 1.—Example of the full-sky spherical harmonic and the related cut-sky orthonormal functions (Górski 1994) used in Fourier analysis of the DMR and foreground emission template data. One function, indexed $l = 7$, $m = -3$, out of the full set of 961 is shown. Note the coordinate frame and Galaxy cut dependence.

which render the maximum likelihood solutions $\hat{\alpha}_\nu^k$. The parameter covariance matrix [dimension $(M \times N)^2$] is

$$M^{-1}_{\alpha\alpha'} \equiv -\frac{\partial^2 \ln P}{\partial \alpha_\nu^k \, \partial \alpha_{\nu'}^{k'}} = \boldsymbol{f}_k^{\mathrm{T}} \cdot (\boldsymbol{C}^{-1}_{\mathrm{SN}\Theta})_{\nu\nu'} \cdot \boldsymbol{f}_{k'} \,. \tag{7}$$

In both equations $(\boldsymbol{C}^{-1}_{\mathrm{SN}\Theta})_{\nu\nu'}$ is a square portion of the inverse covariance matrix $\boldsymbol{C}^{-1}_{\mathrm{SN}\Theta}$ acting between frequencies ν and ν'.

We apply this formalism to study the sensitivity of parameterization of the cosmological CMB anisotropy derived from the DMR data to the possible contamination by high-latitude Galactic foreground emission. We assume that the faint foreground glow of synchrotron, free-free, and dust emission outside the Galactic plane can be traced by the available templates from observations at frequencies in which the CMB does not dominate. Two plausible selections (Kogut et al. 1996a, 1996b) are the DIRBE 140 μm data (Reach et al. 1995) and the 408 MHz full sky radio map (Haslam et al. 1980). (We also used the 110 and 240 μm DIRBE data and found the coupling of these to the DMR frequencies indistinguishable from that derived at 140 μm.) We conduct the analysis as outlined above with $M = 3$ DMR frequencies and $N = 2$ templates. Together with the CMB parameters Q and n this constitutes an eight-dimensional likelihood problem. (An extension of this method is used in Banday et al. 1996b to cross-correlate the DMR data with existing catalogs of extragalactic objects; there we have employed $N = 6$ templates and solved the 20-dimensional likelihood problem.) For each Galaxy cut selection we evaluate the Q-n likelihood, both without and with the foreground correction applied to the data. At each Q-n grid point we derive the maximum likelihood solutions $\hat{\alpha}_\nu^i(Q, n)$ (and their covariance matrix), and use these values to compute the foreground corrected likelihood. Maximizing the corrected likelihood renders simultaneously the most likely solution for both the cosmological (Q-n) and foreground ($\hat{\alpha}_\nu^i$) fitting problem. Figure 2 shows the Q-n likelihood averaged values of the six coupling constants between the three DMR maps and the 140 μm and 408 MHz data. The derived foreground couplings depend only weakly on map pixelization and Galaxy cut. The inferred contributions of Galactic dust, free-free, and synchrotron emission to the high-latitude DMR sky maps are small. (Their physical interpretation is discussed by Kogut et al. 1996a, 1996b.) Here we proceed to discuss the primary target of the analysis of the foreground corrected DMR sky maps—the cosmic CMB anisotropy.

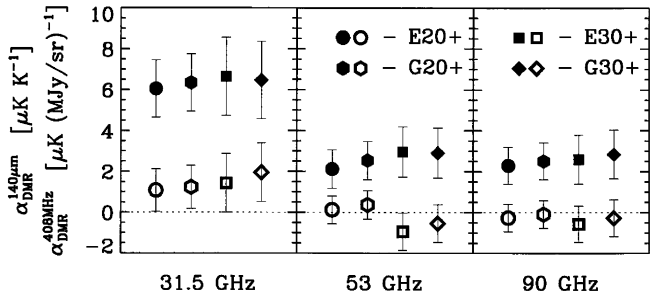

FIG. 2.—Coefficients of coupling between the three DMR channels at 31.5, 53, and 90 GHz and the Galactic templates: the 140 μm DIRBE data (*filled symbols*), and the 408 MHz radio data (*open symbols*). The coefficients shown in the plot (computed for the choice of pixelization and Galaxy cut as indicated) are the maximum likelihood values averaged over the (Q-n) likelihood of the simultaneous background and foreground fit to the 4 yr DMR data. The 1 σ confidence intervals are defined in the usual manner as the square roots of the diagonal on the covariance matrix.

4. RESULTS

Likelihood analysis of the 4 yr DMR data was conducted in both ecliptic and Galactic pixelization with a variety of Galaxy cuts, with and without corrections for the diffuse Galaxy emission. The aim of this analysis was to study the robustness of the derived parameterization of the power spectrum of cosmological CMB anisotropy. A summary of the results of this study is as follows.

Figure 3 (Plate L7) shows the co-added, foreground-corrected DMR sky maps in both the ecliptic and Galactic coordinate pixelization. For visualization the maps have been "cleaned" by removing the $\ell > 40$ noise (the 7° FWHM DMR beam picks up sky signals that are entirely contained within $\ell \leq 40$ in Fourier space). Ecliptic and Galactic maps are very consistent at large angular scales, but near the pixel scale the localized effects of the reference frame–dependent data binning are noticeable. The choice of pixelization rebins roughly half of the instrument noise while leaving the CMB anisotropy nearly unchanged (because of the small ratio of pixel to beam size); consequently, slight variations in the likelihood results are expected.

Figure 4 displays the cut-sky DMR power spectra before and after the foreground correction evaluated for four combinations of pixelization and Galaxy cut. (These spectra are shown here for illustration purposes only; the likelihood method uses the Fourier coefficients c_i, not any quadratic function thereof.) An important result of the simultaneous CMB background (Q, n) and foreground (α_ν^k) fitting to DMR data is that the Galaxy correction affects only the very low order multipoles of the derived cosmic CMB anisotropy. Since the quadrupole moment of the Galaxy is partially counteraligned to the CMB quadrupole (Kogut et al. 1996b), correcting the DMR maps for Galactic emission *increases* the estimated CMB quadrupole.

Table 1 provides a summary of the maximum likelihood solutions for the CMB anisotropy power spectrum model parameters. The first entries refer to the high-latitude co-added DMR maps from which no model of Galactic emission has been removed. For comparison with the published 2 yr analyses, the results of reapplication of the $|b| = 20°$ Galaxy cut are included. One should note the following: (1) Compared to the G20 2 yr results (G94b) the 4 yr DMR data render a slightly smaller, but statistically consistent, power spectrum normalization (roughly a $\sim$0.5 μK drop of $Q|_{n=1}$). (2) Solutions for n are fairly stable with respect to variation of the Galaxy cut, but the derived anisotropy amplitude decreases by more than 1 μK upon removal of the bright Scorpius-Ophiucus and Taurus-Orion foreground regions (i.e., upon extension of Galaxy cut from 20 to 20+). (3) An extra, but smaller, decrease of the amplitude results from a further extension of Galaxy cut (to 30+); we consider this as suggestive of having reached a sufficiently deep Galaxy plane excision with the 20+ cut. Certainly the higher Galactic cut excludes real CMB features correlated over large areas of the sky in the range $20° < |b| < 30°$, which affects the Q-n fits. Comparing results for which the quadrupole is included ($\ell_{\mathrm{min}} = 2$) to those from which it has been excluded ($\ell_{\mathrm{min}} = 3$), we find again a systematic shift to higher normalization and lower index n in the quadrupole-excluded results. The shift is well within the uncertainties from noise and cosmic variance, but reflects at least in part the counteralignment of the CMB and Galactic

PLATE L7

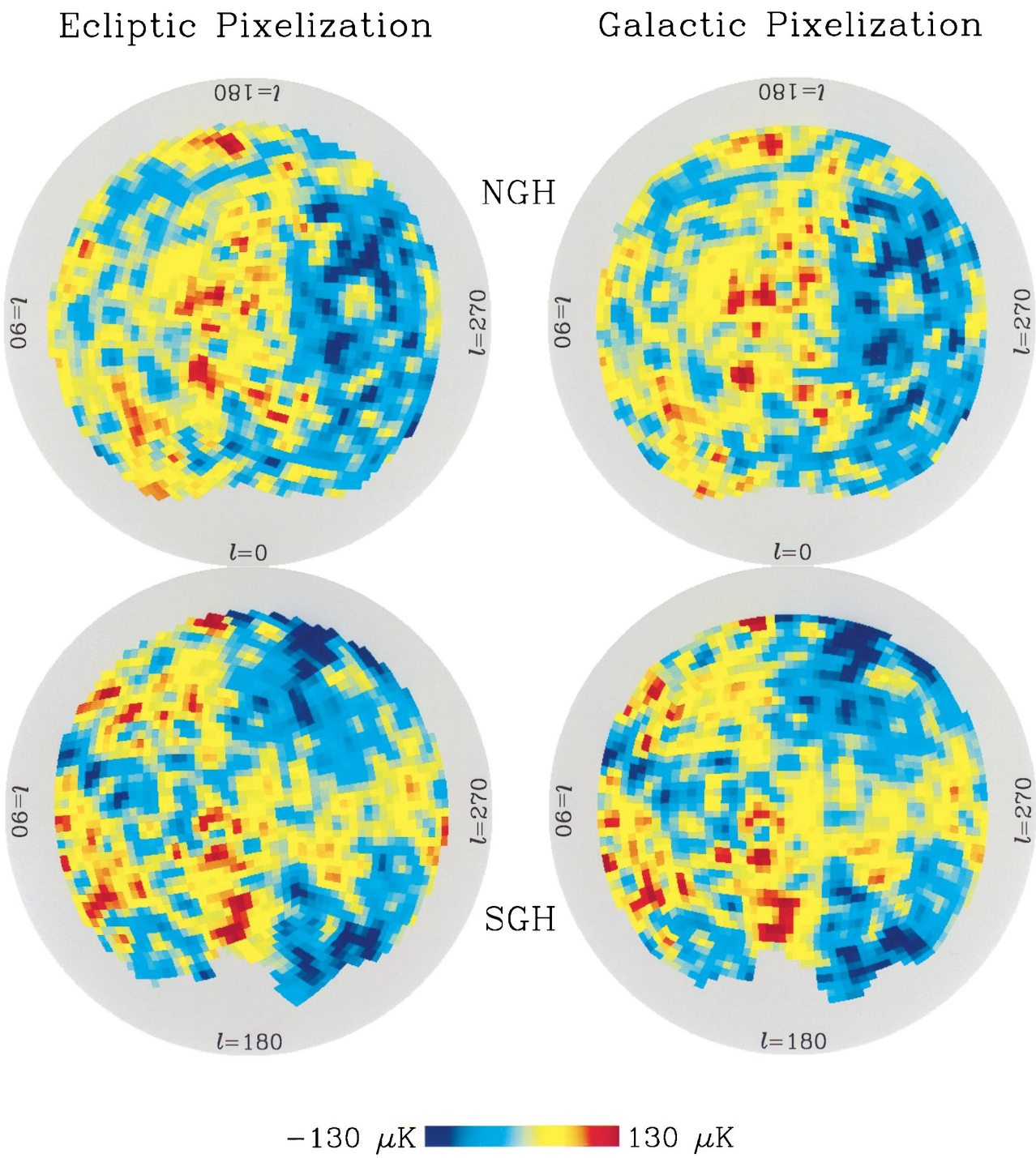

FIG. 3.—*COBE* DMR 4 yr, 31.5, 53, and 90 GHz sky maps co-added after foreground correction according to the 140 μm and 408 MHz template fitting. Galactic and ecliptic (rotated to Galactic coordinates to facilitate the comparison) pixelizations are shown. NGH and SGH denote north and south Galactic hemisphere, respectively. Gray areas mask the maps in the region of extended Galaxy cuts (E20+ and G20+ cuts are shown). Noise reducing Fourier removal of the $l > 40$ content of the raw data has been applied to the full sky maps in order to aid visualization. However, in the rms-per-pixel sense, the displayed maps are still moderately noise dominated (S/N ~ 0.9). Apparent small differences in pixel temperatures are induced by the reference frame-dependent time-ordered data binning in the map making procedure.

GÓRSKI et al. (see 464, L13)

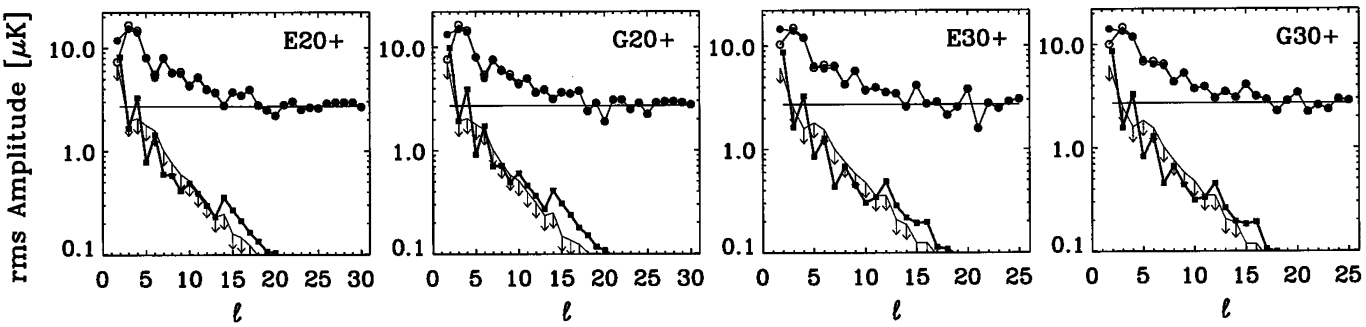

FIG. 4.—Power spectra of the co-added DMR data and the templates used to assess the Galactic foreground emission. The four panels exhibit the cut-sky power spectra, $c_l \equiv [(\sum_{i=l^2+1}^{i=(l+1)^2} c_i^2)/(2l+1)]^{1/2}$, evaluated for both ecliptic and Galactic data with two Galaxy cuts as indicated. (c_ℓ is used in the definition of the cut-sky spectrum to avoid confusion with commonly used C_ℓ symbols, which denote the theoretical, full-sky anisotropy spectrum.) *Open circles*—co-added raw DMR data; *filled circles*—foreground corrected DMR data; *filled squares*—foreground emission contribution to the DMR 53 GHz data characterized by spatial structure of the 140 μm DIRBE map; *arrows*—95% upper limit to possible foreground emission in the DMR 53 GHz channel characterized by spatial structure of the 408 MHz radio data; *horizontal lines*—rms noise per Fourier mode in the co-added 4 yr DMR maps.

quadrupoles: if the quadrupole is to be retained in the inference of cosmological parameters, Galactic emission should be accounted for in the data.

The next set of entries in Table 1 refers to the DMR maps corrected for Galactic emission using the 408 MHz survey to trace synchrotron emission and the DIRBE 140 μm map to trace dust and free-free emission. The linear combination map has any leftover free-free emission removed (eq. [2]), but it is relatively noisy compared to the co-added maps, which is reflected in lower significance of the derived parameters. In the analysis of maximally sensitive, co-added, foreground corrected DMR maps, the residual free-free emission (whose spatial distribution does not follow the 140 μm template) is ignored. The fitted values for Q and n are in good agreement for both foreground correction techniques. One will note that the high-latitude foreground correction reduces the fitted power spectrum amplitude by only $\sim$0.5 μK. This is marginally significant, particularly in the light of a discrepancy between the results derived from the Galactic and ecliptic maps, and especially in comparison with an overall statistical significance of the determined parameters.

Table 1 clearly shows that derived power spectrum parameters vary little with changes in the map pixelization, Galaxy cut, and method of foreground modeling. Since it would be difficult to argue convincingly for any of the tabulated results to be preferred over any other, a judgment call is required to

TABLE 1

DERIVED PARAMETERS FROM THE LIKELIHOOD ANALYSIS OF *COBE* DMR FOUR-YEAR SKY MAPS[a]

		PIXELIZATION/GALAXY CUTS					
l_{min}	PARAMETER	E20	E20+	E30+	G20	G20+	G30+
Co-added Map: No Galaxy Correction							
2	n	$1.13^{+0.26}_{-0.27}{}^{+0.50}_{-0.55}$	$1.22^{+0.24}_{-0.28}{}^{+0.47}_{-0.56}$	$1.24^{+0.30}_{-0.29}{}^{+0.57}_{-0.62}$	$1.22^{+0.24}_{-0.28}{}^{+0.48}_{-0.57}$	$1.23^{+0.23}_{-0.29}{}^{+0.47}_{-0.58}$	$1.23^{+0.29}_{-0.34}{}^{+0.55}_{-0.68}$
	Q	$18.25^{+4.46}_{-3.31}{}^{+10.4}_{-5.94}$	$15.90^{+3.93}_{-2.73}{}^{+9.01}_{-4.99}$	$14.99^{+3.93}_{-3.02}{}^{+9.54}_{-5.23}$	$16.71^{+3.93}_{-3.12}{}^{+9.30}_{-5.47}$	$15.26^{+3.93}_{-2.64}{}^{+8.96}_{-4.84}$	$15.18^{+4.46}_{-2.92}{}^{+10.5}_{-5.27}$
	$Q\|_{n=1}$	$20.16^{+1.34}_{-1.25}{}^{+2.83}_{-2.44}$	$18.73^{+1.25}_{-1.20}{}^{+2.64}_{-2.35}$	$17.96^{+1.44}_{-1.34}{}^{+3.02}_{-2.64}$	$19.40^{+1.29}_{-1.25}{}^{+2.78}_{-2.44}$	$18.34^{+1.25}_{-1.20}{}^{+2.64}_{-2.35}$	$17.82^{+1.44}_{-1.34}{}^{+3.02}_{-2.64}$
3	n	$0.96^{+0.28}_{-0.30}{}^{+0.54}_{-0.63}$	$1.00^{+0.28}_{-0.29}{}^{+0.54}_{-0.61}$	$1.01^{+0.32}_{-0.35}{}^{+0.63}_{-0.72}$	$1.02^{+0.28}_{-0.29}{}^{+0.54}_{-0.62}$	$0.99^{+0.28}_{-0.30}{}^{+0.54}_{-0.62}$	$0.93^{+0.34}_{-0.36}{}^{+0.66}_{-0.75}$
	Q	$20.98^{+6.04}_{-4.12}{}^{+14.2}_{-7.33}$	$19.11^{+5.08}_{-3.84}{}^{+12.2}_{-6.71}$	$18.30^{+5.80}_{-4.17}{}^{+14.3}_{-7.19}$	$19.40^{+5.23}_{-4.03}{}^{+12.7}_{-7.00}$	$18.82^{+4.89}_{-3.88}{}^{+12.0}_{-6.76}$	$19.01^{+6.38}_{-4.41}{}^{+15.6}_{-7.53}$
	$Q\|_{n=1}$	$20.50^{+1.34}_{-1.29}{}^{+2.83}_{-2.54}$	$19.11^{+1.25}_{-1.25}{}^{+2.68}_{-2.40}$	$18.44^{+1.49}_{-1.39}{}^{+3.12}_{-2.73}$	$19.73^{+1.34}_{-1.25}{}^{+2.83}_{-2.49}$	$18.68^{+1.29}_{-1.20}{}^{+2.68}_{-2.40}$	$18.30^{+1.49}_{-1.39}{}^{+3.12}_{-2.68}$
Linear Combination Map							
2	n		$1.29^{+0.34}_{-0.43}{}^{+0.69}_{-0.87}$	$1.19^{+0.46}_{-0.55}{}^{+0.88}_{-1.14}$		$1.11^{+0.38}_{-0.42}{}^{+0.73}_{-0.87}$	$0.79^{+0.48}_{-0.55}{}^{+0.92}_{-1.07}$
	Q		$15.75^{+5.08}_{-3.45}{}^{+12.3}_{-6.09}$	$15.80^{+6.57}_{-4.08}{}^{+16.3}_{-7.05}$		$16.33^{+5.18}_{-3.69}{}^{+12.8}_{-6.38}$	$18.63^{+7.72}_{-5.08}{}^{+18.8}_{-8.58}$
	$Q\|_{n=1}$		$18.58^{+1.87}_{-1.73}{}^{+3.88}_{-3.40}$	$17.53^{+2.06}_{-1.87}{}^{+4.36}_{-3.64}$		$17.38^{+1.77}_{-1.68}{}^{+3.74}_{-3.74}$	$16.57^{+1.92}_{-1.82}{}^{+4.08}_{-3.50}$
Co-added Map: Galaxy Corrected							
2	n		$1.24^{+0.23}_{-0.29}{}^{+0.47}_{-0.57}$	$1.24^{+0.29}_{-0.29}{}^{+0.55}_{-0.62}$		$1.21^{+0.24}_{-0.28}{}^{+0.48}_{-0.57}$	$1.24^{+0.27}_{-0.33}{}^{+0.54}_{-0.67}$
	Q		$15.47^{+3.55}_{-2.78}{}^{+8.39}_{-4.94}$	$14.80^{+3.79}_{-2.88}{}^{+9.06}_{-5.03}$		$15.23^{+3.69}_{-2.64}{}^{+8.58}_{-4.75}$	$14.80^{+4.07}_{-2.83}{}^{+9.64}_{-5.08}$
	$Q\|_{n=1}$		$18.20^{+1.25}_{-1.20}{}^{+2.59}_{-2.35}$	$17.48^{+1.44}_{-1.34}{}^{+3.02}_{-2.59}$		$17.67^{+1.25}_{-1.15}{}^{+2.59}_{-2.30}$	$17.34^{+1.39}_{-1.34}{}^{+2.97}_{-2.59}$

[a] We derive the tabulated values for Q and n by projecting the two-dimensional, Q-n likelihood function onto the Q- or n-axis (rather than marginalizing) and quote the maximal likelihood value and the 68% and 95% credible intervals of the resulting one-dimensional likelihood densities. We also evaluate the likelihood along the slice at $n = 1$ to derive the CMB anisotropy normalization for an exact Harrison-Zeldovich power spectrum.

quote a unique *COBE* DMR determination of the primordial power spectrum parameters. A representative summary of the present results is as follows: The 4 yr data are *consistent* with quadrupole normalization $Q_{\rm rms-PS} \sim 15.3^{+3.7}_{-2.8}$ μK and power-law index $n \sim 1.2 \pm 0.3$. With n fixed at unity, we infer the normalization for an exact scale-invariant Harrison-Zeldovich power spectrum $Q_{\rm rms-PS}|_{n=1} \sim 18$ μK with high ($\gtrsim 14$ σ) significance $\delta Q/Q \lesssim 0.07$. Implications of the *COBE* DMR 4 yr data for the specific models of large-scale structure formation will be discussed elsewhere.

We gratefully acknowledge the efforts of those contributing to the *COBE* DMR. *COBE* is supported by the Office of Space Sciences of NASA Headquarters.

REFERENCES

Banday, A. J., et al. 1996a, ApJ, submitted
———. 1996b, ApJ, submitted
Bennett, C. L., et al. 1992, ApJ, 396, L7
———. 1996, ApJL, 464, L1
Bond, J. R., & Efstathiou, G. 1987, MNRAS, 226, 655
de Vaucouleurs, G. 1956, Vistas Astron., 2, 1584
Fabbri, R., Lucchin, F., & Matarrese, S. 1987, ApJ, 315, 1
Górski, K. M. 1994, ApJ, 430, L85 (G94a)
Górski, K. M., et al. 1994, ApJ, 430, L89 (G94b)
———. 1996, in preparation
Haslam, C. G. T., et al. 1981, A&A, 100, 209
Kogut, A., Banday, A. J., Bennett, C. L., Górski, K. M., Hinshaw, G., & Reach, W. T. 1996a, ApJ, 460, 1
Kogut, A., Banday, A. J., Bennett, C. L., Górski, K. M., Hinshaw, G., Smoot, G. F., & Wright, E. L. 1996b, 464, L5
———. 1996c, 464, L29
Kogut, A., et al. 1992, ApJ, 401, 1
Lineweaver, C., et al. 1994, ApJ, 436, 452
Reach, W. T., Franz, B. A., Kelsall, T., & Weiland, J. L. 1995, Unveiling the Cosmic Infrared Background, ed. E. Dwek (New York: AIP), 37
Smoot, G. F., et al. 1992, ApJ, 396, L1
Wright, E. L., et al. 1992, ApJ, 396, L13